Solid versus solution: Examining the electronic structure of metallic DNA with soft x-ray spectroscopy

J. B. MacNaughton,[1,*] M. V. Yablonskikh,[1,2] A. H. Hunt,[1] E. Z. Kurmaev,[2] J. S. Lee,[3] S. D. Wettig,[4] and A. Moewes[1]
[1]*Department of Physics and Engineering Physics, University of Saskatchewan, 116 Science Place, Saskatoon, Saskatchewan, Canada S7N 5E2*
[2]*Institute of Metal Physics, Russian Academy of Sciences Ural Division, 620219 Yekaterinburg GSP-170, Russia*
[3]*Department of Biochemistry, University of Saskatchewan, 107 Wiggins Road, Saskatoon, Saskatchewan, Canada S7N 5E5*
[4]*College of Pharmacy and Nutrition, University of Saskatchewan, 110 Science Place, Saskatoon, Saskatchewan, Canada S7N 5C9*
(Received 5 July 2006; published 6 September 2006)

Soft x-ray spectroscopy is used to investigate solution and powder samples of (Ni)·*M*-DNA. The nickel 2*p* absorption spectra are representative of the metal-DNA interaction, and they are not dominated by residual nickel structures. Both solution and solid samples of (Ni)·*M*-DNA contain a high spin Ni(II) configuration. Differences in the electronic structures of the solution and powder, an 8.2 eV loss process, and variations in hydrogen bonding are discussed. It is found that the drying process alters the electronic structure of the metallic DNA sample.

DOI: 10.1103/PhysRevB.74.125101 PACS number(s): 71.20.Rv, 78.70.En, 78.70.Dm, 71.15.Mb

I. INTRODUCTION

The idea of using DNA in the production of nanoelectronic devices has prompted investigations into its electronic properties.[1] While a highly conductive form of DNA would be an ideal material for self-assembling nanocircuits, it has so far been elusive. Contradictory studies of the electrical properties of DNA have reported conductivity ranging from insulating,[2–5] semiconducting,[6–8] highly conductive,[9] to superconducting.[10] Possible causes for the varying conductivity include differences in experimental setup, the complexity of the DNA structure, and variations in synthesis techniques, including the effects of drying the DNA samples. The last two topics are addressed in this study.

Altering the distribution of water and ions in the local chemical environment of the DNA helix has been shown to influence both the physical and electronic structure of DNA.[11–13] Biomaterials of interest for nanoelectronics are often prepared in solution, and then dried to a solid-state form. Modifications to the physical and electronic structures as a result of this phase transition are significant, and understanding these changes is crucial in determining how to tailor biomaterials in a reproducible way. Specific knowledge is limited due to difficulties in designing experiments to analyze the electronic structure of both solution and solid samples without considerable changes in experimental setup, which may ultimately affect the experiment's outcome.

The local chemical environment differs for molecules in solution and in solid form. Significant differences in the electronic structures of the liquid and solid phases of water have been found.[14] When DNA is lyophilized, the local ions and water molecules are no longer dynamic, and more rigid bonds replace the constant reorganization of bonding that is possible in solution form. *B*-DNA (base pair separation of 3.4 Å and twist angle of 36°) is the most well known structural form of DNA under conditions of high water content, while the *A*-DNA structure (base pair separation of 2.5 Å and twist angle of 32.7°) is favored under dryer conditions.[15] Either *A*-DNA or a combination of *A* and *B* DNA may be favorable in dry DNA, because of lower humidity. It is found that the concentration and size of cations in the local chemical environment are important in initiating structural phase transitions in DNA.[13]

Attempts have been made to improve the electron transport properties of DNA by incorporating metal ions into the structure or growing metal on the surface.[16] A method of integrating metal into the structure, while preserving the desirable properties of the DNA helix, is to convert *B*-DNA to (*X*)·*M*-DNA by the addition of divalent metal ions (Zn^{2+}, Co^{2+}, or Ni^{2+}) at pH values above 8.5.[17] Investigations of the conductivity have shown that (Zn)·*M*-DNA is more efficient at electron transfer than *B*-DNA,[18] and recent studies have focused on investigating the electronic structure of powder[19] [(*X*)·*M*-DNA, *X*=Ni, Co] and thin film[20] [(*X*)·*M*-DNA, *X*=Mn, Ca, Zn; although it has been previously reported that *M*-DNA will not form with Mn^{2+} and Ca^{2+} ions[17]] metallic DNA systems.

Soft x-ray absorption (XAS) and emission (XES) spectroscopy directly examines the occupied and unoccupied partial densities of states without the difficulties of a microscopic setup that may affect the system being investigated. We present a spectroscopic study of the electronic structure and the interaction of metal ions with DNA in both solution and powder samples of (Ni)·*M*-DNA with minimal change in experimental setup. X-ray absorption spectra are compared to density functional theory (DFT) calculations of model compounds to determine the origin of spectral contributions. Nickel *L* edge resonant inelastic soft x-ray scattering (RIXS) measurements demonstrate the differences between the occupied states in the solid and solution.

II. SAMPLE PREPARATION

Conditions must be carefully controlled during sample preparation to allow for (*X*)·*M*-DNA to form. If the pH is

too high the metal salts will precipitate from the solution, but if the pH is too low the $(X)\cdot M$-DNA structure will not form.[21] Both the $(Ni)\cdot M$-DNA liquid and powder samples will likely have excess metal ions that are not bonded directly to the DNA strand. The $(Ni)\cdot M$-DNA solution was prepared using a buffer to help stabilize the pH and was split into two parts; one portion was used for the solution sample, while the other was lyophilized. A concentrated DNA stock solution ($\sim$1.5 mg/mL) was prepared and diluted to a final concentration of 100 μg/mL. The DNA was sheared by five passages of the stock solution through a syringe needle.[22] The $(Ni)\cdot M$-DNA samples were prepared using tris(hydroxymethyl)aminomethane (TRIS) buffer (pH adjusted with HCl) and 0.1 mM $NiCl_2$ at pH 8.5 according to the technique previously described[17,21] Calf thymus DNA (42% G-C, 58% A-T) and the TRIS buffer were purchased from Sigma. Metal chloride salts were obtained from Aldrich.

III. EXPERIMENTAL

All measurements were performed using the soft x-ray fluorescence end station at Beamline 8.0.1 at the Advanced Light Source.[23] The x-ray absorption spectra were measured in partial fluorescence yield (PFY) mode, with the spectrometer window set to monitor the Ni $L_{2,3}$ emission (from 783 to 933 eV). The resolution was about 0.25 eV for the Ni $2p$ XAS, and 2.2 eV FWHM for the Ni $L_{2,3}$ XES measurements. Absorption of the liquid cell window, the liquid sample environment, and the diluted metal concentration in the DNA samples all contributed to the requirement for high photon flux, limiting the experimental resolution.

The $(Ni)\cdot M$-DNA solution was placed into the UHV sample chamber inside a liquid cell with a 1 mm$\times$1 mm $\times$100 nm thick Si_3N_4 window.[24] The nickel L edge was chosen to analyze the metal-DNA interaction because photon energies do not coincide with Si or N absorption edges of the window. All samples were mounted on the same sample holder to allow measurements to be made consecutively, with the same experimental geometry (90° between the incoming photon beam and the spectrometer).

IV. CALCULATIONS

X-ray absorption spectra have been simulated using the StoBe software.[25] A transition state approximation with a half-occupied core hole at the location of the excitation was used.[26] The oscillator strengths for transitions from the core level to the unoccupied excited state orbitals were calculated, then broadened with Gaussian functions with linewidths of 1.0 eV (FWHM) up to the ionization potential and then linearly increasing to 4.0 eV (FWHM) over the next 10 eV. These linewidths were chosen to correspond to the experimentally observed results. In all cases the theoretical spectra have been shifted in energy to align with the experimental data. The minimum intensity value has been set to zero for all spectra. Triple-zeta plus valence polarization (TZVP) Huzinaga orbital basis sets and $A5$ auxiliary basis sets were used.[27]

In our models, three molecules were selected to represent some possible residual metal structures that could be present due to the metal ions not directly bonded to the DNA. Nickel chloride was included because it was added to the solution to provide metal ions during sample preparation. The metal oxides NiO and NiOH represent other possible structures that may form through interactions with the buffer solution. These selections are not intended to represent all possible structures that could exist in the sample, just some of the common ones. Models of the NiO, $(NiOH)^+$, and $NiCl_2$ molecules were first created using the Spartan 04 program,[28] and then optimized using StoBe.

The large number of atoms in DNA results in challenges when developing analytical and theoretical approaches, and so simpler systems are used to model the more complicated picture. To determine spectral contributions from the metal-DNA interaction, it was necessary to create a model of the nucleobases of $(X)\cdot M$-DNA. A proposed structure of $(X)\cdot M$-DNA shows a metal ion replacing the hydrogen atom at the $N3$ position of thymine and the $N1$ position of guanine of every base pair, which is supported by NMR measurements,[21] but not yet confirmed by crystallographic data. In general, the $N7$ sites of guanine and adenine are preferable metal binding sites,[29,30] however a modified adenine-thymine base pair with the proton at the $N3$ location of thymine replaced with a Pt(II) ion has been found for the mixed 1-methylthymine, 9-methyladenine complex of *trans*-$[Pt(II)(NH_2Me)_2]$.[29] Metal ion interactions with the $N3$ site are possible but less prevalent than bonding with the $N7$ site; however if an increase in pH effectively deprotonates the $N3$ site, this may increase the likelihood of a metal ion binding at that site.[30]

Previous DFT calculations of a Zn(II) guanine-cytosine M-DNA nucleobase pair were attempted but it was difficult to find a planar equilibrium structure.[31] This may indicate problems with the model, or that including the effect of stacking interactions is important when optimizing the structure. We desired to calculate the effects of the metal-nucleobase interaction on the electronic structure and have chosen to use the originally proposed model.[21] Hydrogen atoms at the $N3$ position of thymine and the $N1$ position of guanine were replaced with a nickel ion and the Watson-Crick nucleobases were allowed to rotate by 20° around an axis perpendicular to the plane of the nucleobases, to allow the bond length between the Ni and the N to increase to 2 Å,[17] as displayed in Fig. 1. XAS spectra were calculated for the nickel adenine-thymine (Ni-AT) and nickel guanine-cytosine (Ni-GC) nucleobase pairs using StoBe.

V. RESULTS AND DISCUSSION

Nickel $2p$ absorption spectroscopy has proven useful for examining the electronic structure of biological systems, in particular determining the oxidation states and spin states of nickel containing enzymes.[32,33] The Ni $2p$ spin orbit interaction splits the spectrum into two sections, which consist of the $2p_{3/2}$ (L_3) and the $2p_{1/2}$ (L_2) features. The multiplet structure in the nickel spectra is the result of the Coulomb and exchange interactions between the $3d$ shell and the core hole.

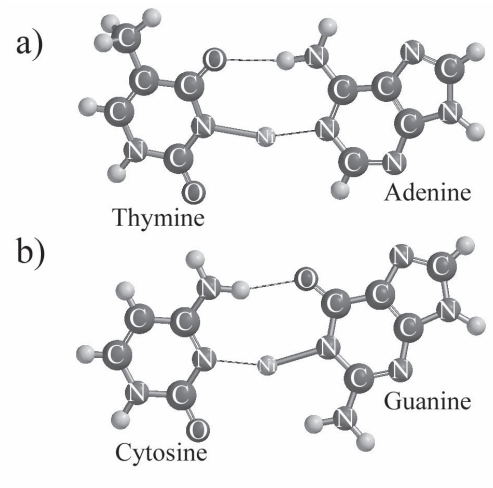

FIG. 1. Molecular structure of the nickel containing metallic DNA nucleobase pairs used for calculations. Part (a) displays the adenine-thymine nucleobase pair (Ni-AT), while part (b) shows the cytosine-guanine nucleobase pair (Ni-GC).

This fine structure can reveal information about the nickel oxidation state and, specifically for the Ni(II) state, distinguish between the $3d$ (Ref. 8) high and low spin configurations.[34] It is found that Ni(I) spectra exhibit no multiplet structure due to a full d shell in the final state, high spin Ni(II) spectra have multiplet structure on the high energy slope of the L_3 peak and a broad or split L_2 edge, low spin Ni(II) spectra have minimal multiplet features on the L_3 peak and a sharper L_2 edge, ionic Ni(III) multiplet features are found on the low energy side of the L_3 peak, and covalently bonded Ni(III) has broad features lacking multiplet structure.[32] The measured spectra in Fig. 2 clearly show multiplet structure on the high energy side of the L_3 peak, indicating a high spin Ni(II) configuration for both the solution and powder (Ni)·M-DNA samples. This configuration may lead to octahedral, tetrahedral, or square planar symmetry.

The spectra of the solution and powder samples of (Ni)·M-DNA have richer structures than the spectra of nickel metal in Fig. 2. This is because the $2p \rightarrow 3d$ multiplet structure reflects the behavior of the $3d$ orbitals in the presence of ligands,[34] which applies to both molecular environments, but not to the metal. Feature A in the experimental spectra is the main peak associated with the $2p_{3/2}$ absorption edge and is well represented in the theoretical spectra. While the interaction of nickel with oxygen likely influences both feature B and C in the spectra when comparing the theoretical spectra of NiO and NiOH to experiment, the influence of the excess $NiCl_2$ is minimal. The calculations of these simple compounds suggest that the spectra are not dominated by contributions from residual nickel compounds; rather they represent a combination of the excess nickel structures and the metal-DNA interaction. Feature C is seen in the calculated spectra of Ni-GC and Ni-AT, indicating that the electronic structure is influenced by the metal-DNA interaction. This feature is prominent in the (Ni)·M-DNA powder spectrum, but not in the spectrum for the solution sample. This is possibly due to dilution effects in the solution or to differences in the ligands associated with the nickel ions.

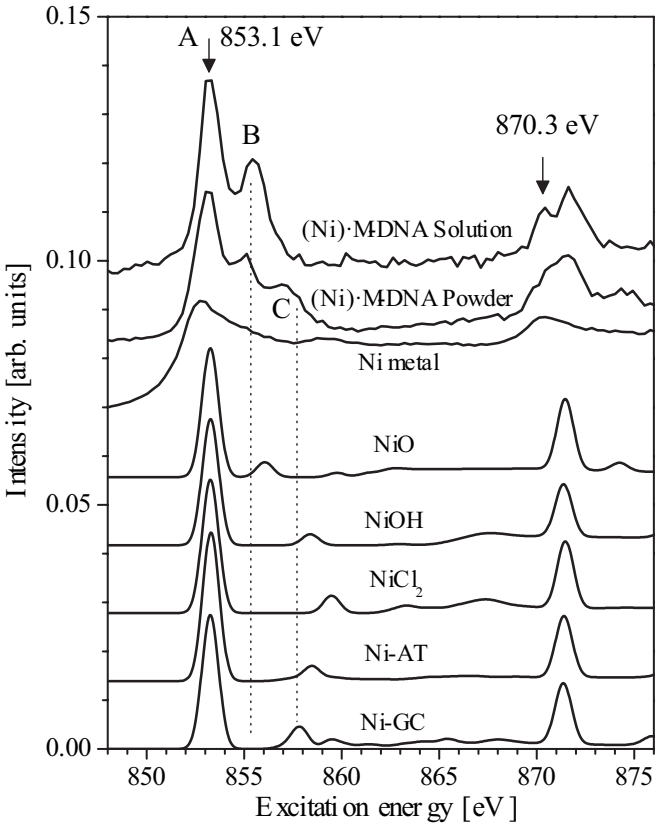

FIG. 2. Experimental Ni $2p$ XAS spectra of the (Ni)·M-DNA solution, (Ni)·M-DNA powder, and Ni metal are compared with theoretical spectra of NiO, NiOH, $NiCl_2$, Ni-AT, and Ni-GC. The experimental spectra were measured in partial fluorescence yield (PFY) mode.

Resonant soft x-ray emission spectra [excited at L_2 (a) and L_3 (b) thresholds] are displayed in Fig. 3. Both the solution and powder (Ni)·M-DNA $L_{2,3}$ emission are shifted higher in energy from the nickel metal spectrum due to the chemical shift of $2p$ core levels typical in Ni(II) compounds. This shift ranges from 0.6 eV in the nonresonant case (not shown), to 1.4 eV when excited on the L_2 threshold, to 1.6 eV when excited on the L_3 threshold. The metal spectra remain at constant emission energy.

The integral intensity ratio $I(L_2)/I(L_3)$ provides information concerning the population of the valence states of $3d$ and $4s$ symmetry. Neglecting the effects of nonradiative transitions, this intensity ratio should be equal to $\frac{1}{2}$ for free atoms. The electrostatic interaction between $2p$ core holes and electrons in the unfilled $3d$ shell can cause this ratio to change from the value of $\frac{1}{2}$ when free $3d$ atoms are condensed into a solid. Furthermore, nonradiative $L_2L_3M_{4,5}$ Coster-Kronig (C-K) transitions also influence the $I(L_2)/I(L_3)$ ratio in $3d$ metal solids.[35] Generally, C-K transitions partially depopulate the L_3 state when nonradiative transitions from the L_3 to the L_2 level occur before the emission process.

Changes in the $I(L_2)/I(L_3)$ intensity ratio are established in Fig. 3(a). It is found that the measured integral intensity ratio $I(L_2)/I(L_3)$ increases from the Ni metal (0.27), to the

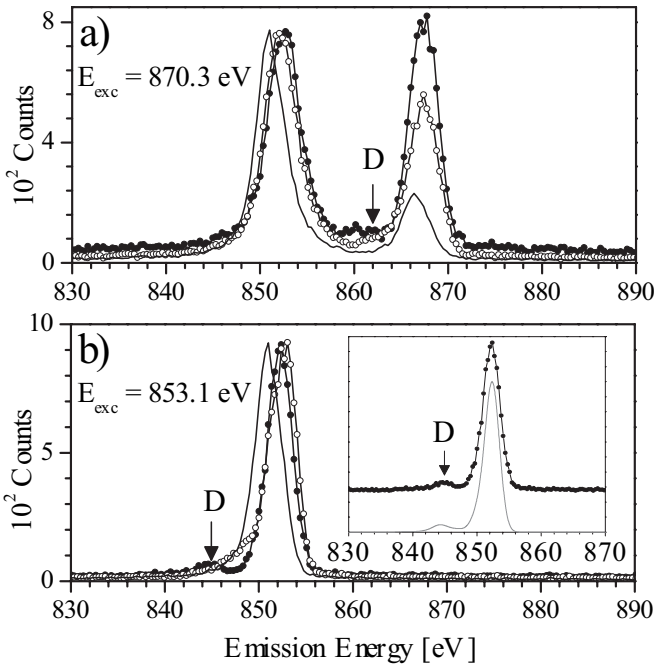

FIG. 3. $L_{2,3}$ RIXS spectra of the (Ni)·*M*-DNA solution (solid dots), (Ni)·*M*-DNA powder (hollow dots), and Ni metal (solid line). Part (a) shows resonant emission spectra when excited on the L_2 threshold, and (b) displays resonant emission spectra when excited on the L_3 threshold. The inset shows the (Ni)·*M*-DNA liquid spectrum (solid dots) from part (b) compared to a RIXS calculation of Ni^{2+} (gray line).

powder (Ni)·*M*-DNA sample (0.58), to the solution of (Ni)·*M*-DNA (0.81), indicating that the localization of the electronic states also increases. Both the 2*p*-3*d* electrostatic interaction and nonradiative C-K transitions can reduce the ratio for the (Ni)·*M*-DNA powder sample, although not as much as the nickel metal.

A key difference between the solution and powder sample is the arrangement of the hydrogen bonding between the DNA strands and water. It has been found that x-ray spectroscopy is sensitive to the hydrogen bonding in water[14,36] and ice,[14] and the variation in the hydrogen bonding arrangements between the liquid and solid samples result in clear differences in the electronic structure. The ratio change between the two (Ni)·*M*-DNA samples is likely due to a combination of solid state effects such as the 2*p*-3*d* electrostatic interaction and nonradiative C-K transitions in the powder sample, and influences resulting from diversity in the hydrogen bonding networks present in the solution and powder samples.

Feature *D* in Fig. 3 is located 8.2 eV below the excitation energy and is distinct for the solution sample in part (b), and somewhat less pronounced in part (a). The states and dipole transition matrix elements for Ni^{2+} were calculated using the purely atomic Hamiltonian encoded in Cowan's program.[37] The Slater integrals were scaled to 80%. The RIXS calculation was accomplished using the Kramers-Heisenberg formula. The summation of possible transitions over all intermediate states was performed incoherently. The calculations, shown in the inset of Fig. 3 part (b), reveal that the main feature results from normal 3*d* inner shell scattering processes, and feature *D* can be attributed to a $3d \rightarrow 4s$ RIXS transition. To reproduce the experimental spectrum, the intensity of the $3d \rightarrow 4s$ component of the emission spectrum was multiplied by three, indicating that the density of Ni 4*s* states in the solution may be increased through hybridization with ligand states. The $3d \rightarrow 4s$ RIXS transition was broadened to the same FWHM as the 3*d* inner shell scattering transition to correspond to the measured spectrum, indicating that the 4*s* shell is relatively well localized. The powder sample is not well represented by an atomiclike model, and solid state effects including electronic distortions and the Coulomb interaction eliminate the loss process. Loss features in that energy range have traditionally been assigned to charge transfer processes from surrounding *p* ligands.[38]

VI. CONCLUSION

We have described the electronic structure of solution and powder (Ni)·*M*-DNA using nickel *L* edge x-ray absorption and emission spectroscopy, with minimal changes in experimental setup. Comparing nickel 2*p* XAS spectra to calculations it is found that the measurements reflect the interaction of the metal ions with DNA, and are not dominated by excessive metal impurities. Using XAS spectra as fingerprints of nickel coordination, we found that both solution and powder (Ni)·*M*-DNA are high spin Ni(II) compounds. The $I(L_2)/I(L_3)$ intensity ratio in the RIXS spectra is reduced in the powder (Ni)·*M*-DNA compared to the liquid (Ni)·*M*-DNA system due to solid state effects and variations in the hydrogen bonding networks. The presence of an additional feature in the solution RIXS spectra is attributed to energy loss from $3d \rightarrow 4s$ excitations. Drying the metallic DNA sample from solution has a significant effect on the electronic structure.

ACKNOWLEDGMENTS

Funding by the Natural Sciences and Engineering Research Council of Canada (NSERC), the Canada Research Chair Program, the Research Council of the President of the Russian Federation (Grant No. NSH-4192.2006.2), and the Russian Science Foundation for Basic Research (Project 05-02-16438) is gratefully acknowledged. The work at the Advanced Light Source at Lawrence Berkeley National Laboratory was supported by the U.S. Department of Energy (Contract No. DE-AC03-76SF00098).

*Corresponding author. Email address: janay.m@usask.ca

[1] R. G. Endres, D. L. Cox, and R. R. P. Singh, Rev. Mod. Phys. **76**, 195 (2004).
[2] E. Braun, Y. Eichen, U. Sivan, and G. Ben-Yoseph, Nature (London) **391**, 775 (1998).
[3] P. J. de Pablo, F. Moreno-Herrero, J. Colchero, J. Gomez Herrero, P. Herrero, A. M. Baro, P. Ordejon, J. M. Soler, and E. Artacho, Phys. Rev. Lett. **85**, 4992 (2000).
[4] A. J. Storm, J. van Noort, S. de Vries, and C. Dekker, Appl. Phys. Lett. **79**, 3881 (2001).
[5] P. Tran, B. Alavi, and G. Gruner, Phys. Rev. Lett. **85**, 1564 (2000).
[6] D. Porath, A. Bezryadin, S. de Vries, and C. Dekker, Nature (London) **403**, 635 (2000).
[7] K. H. Yoo, D. H. Ha, J. O. Lee, J. W. Park, J. Kim, J. J. Kim, H. Y. Lee, T. Kawai, and H. Y. Choi, Phys. Rev. Lett. **87**, 198102 (2001).
[8] A. Rakitin, P. Aich, C. Papadopoulos, Y. Kobzar, A. S. Vedeneev, J. S. Lee, and J. M. Xu, Phys. Rev. Lett. **86**, 3670 (2001).
[9] H. W. Fink and C. Schönenberger, Nature (London) **398**, 407 (1999).
[10] A. Y. Kasumov, M. Kociak, S. Gueron, B. Reulet, V. T. Volkov, D. V. Klinov, and H. Bouchiat, Science **291**, 280 (2001).
[11] C. Adessi, S. Walch, and M. P. Anantram, Phys. Rev. B **67**, 081405(R) (2003).
[12] A. Hübsch, R. G. Endres, D. L. Cox, and R. R. P. Singh, Phys. Rev. Lett. **94**, 178102 (2005).
[13] T. Weidlich, S. M. Lindsay, and A. Rupprecht, Phys. Rev. Lett. **61**, 1674 (1988).
[14] P. Wernet, D. Nordlund, U. Bergmann, M. Cavalleri, M. Odelius, H. Ogasawara, L. A. Naslund, T. K. Hirsch, L. Ojamae, P. Glatzel, L. G. M. Pettersson, and A. Nilsson, Science **304**, 995 (2004).
[15] K. J. McConnell and D. L. Beveridge, J. Mol. Biol. **304**, 803 (2000).
[16] J. Richter, Physica E (Amsterdam) **16**, 157 (2003).
[17] P. Aich, S. L. Labiuk, L. W. Tari, L. J. T. Delbaere, W. J. Roesler, K. J. Falk, R. P. Steer, and J. S. Lee, J. Mol. Biol. **294**, 477 (1999).
[18] S. D. Wettig, C.-Z. Li, Y.-T. Long, H.-B. Kraatz, and J. S. Lee, Anal. Sci. **19**, 23 (2003).
[19] J. B. MacNaughton, E. Z. Kurmaev, L. D. Finkelstein, J. S. Lee, S. D. Wettig, and A. Moewes, Phys. Rev. B **73**, 205114 (2006).
[20] K. Mizoguchi, S. Tanaka, T. Ogawa, N. Shiobara, and H. Sakamoto, Phys. Rev. B **72**, 033106 (2005).
[21] J. S. Lee, L. J. P. Latimer, and R. S. Reid, Biochem. Cell Biol. **71**, 162 (1993).
[22] R. E. Pyeritz, C. A. Thomas, and R. A. Schlegel, Biochim. Biophys. Acta **272**, 504 (1972).
[23] J. J. Jia, T. A. Callcott, J. Yurkas, A. W. Ellis, F. J. Himpsel, M. G. Samant, J. Stöhr, D. L. Ederer, J. A. Carlisle, E. A. Hudson, L. J. Terminello, D. K. Shuh, and R. C. C. Perera, Rev. Sci. Instrum. **66**, 1394 (1995).
[24] AIP Conf. Proc. **705**, 1066 (2003).
[25] K. Hermann, L. G. M. Pettersson, M. E. Casida, C. Daul, A. Goursot, A. Koester, E. Proynov, A. St-Amant, D. R. Salahub, V. Carravetta, H. Duarte, N. Godbout, J. Guan, C. Jamorski, M. Leboeuf, V. Malkin, O. Malkina, M. Nyberg, L. Pedocchi, F. Sim, L. Triguero, and A. Vela, StoBe-deMon version 2.1, Berlin, 2005.
[26] L. Triguero, L. G. M. Pettersson, and H. Agren, Phys. Rev. B **58**, 8097 (1998).
[27] K. Hermann and L. G. M. Pettersson, Documentation for StoBe2005 (Version 2.1), Berlin, 2005.
[28] Wave function, Inc., Spartan 04, Irvine, CA, 2004.
[29] B. Lippert, J. Chem. Soc. Dalton Trans. **21**, 3971 (1997).
[30] H. Sigel, Chem. Soc. Rev. **22**, 255 (1993).
[31] R. Di Felice, A. Calzolari, and H. Zhang, Nanotechnology **15**, 1256 (2004).
[32] H. X. Wang, C. Y. Ralston, D. S. Patil, R. M. Jones, W. Gu, M. Verhagen, M. Adams, P. Ge, C. Riordan, C. A. Marganian, P. Mascharak, J. Kovacs, C. G. Miller, T. J. Collins, S. Brooker, P. D. Croucher, K. Wang, E. I. Stiefel, and S. P. Cramer, J. Am. Chem. Soc. **122**, 10544 (2000).
[33] H. X. Wang, D. S. Patil, W. W. Gu, L. Jacquamet, S. Friedrich, T. Funk, and S. P. Cramer, J. Electron Spectrosc. Relat. Phenom. **114**, 855 (2001).
[34] G. van der Laan, B. T. Thole, G. A. Sawatzky, and M. Verdaguer, Phys. Rev. B **37**, 6587 (1988).
[35] E. Z. Kurmaev, A. L. Ankudinov, J. J. Rehr, L. D. Finkelstein, P. F. Karimov, and A. Moewes, J. Electron Spectrosc. Relat. Phenom. **148**, 1 (2005).
[36] J. H. Guo, Y. Luo, A. Augustsson, J. E. Rubensson, C. Sathe, H. Agren, H. Siegbahn, and J. Nordgren, Phys. Rev. Lett. **89**, 137402 (2002).
[37] R. D. Cowan, *The Theory of Atomic Structure and Spectra* (University of California Press, Berkeley, 1981).
[38] H. Ishii, Y. Ishiwata, R. Eguchi, Y. Harada, M. Watanabe, A. Chainani, and S. Shin, J. Phys. Soc. Jpn. **70**, 1813 (2001).